25th ABCM International Congress of Mechanical Engineering
October 20-25, 2019, Uberlândia, MG, Brazil

COB-2019-1045
PERFORMANCE COMPARISON OF A SOLAR THERMAL AND A PHOTOVOLTAIC ENERGY SOURCE TO POWER A DESICCANT DRYING SYSTEM

Bruno de Alencar Carneiro
Maria Eugênia Vieira da Silva
Francisco Nivaldo Aguiar Freire
Air Conditioning and Refrigeration Laboratory, Department of Mechanical Engineering, Federal University of Ceará, Fortaleza, CE, Brazil
brunoalnk@hotmail.com
eugenia@ufc.br
nivaldo@ufc.br

Abstract. *The theoretical study compares the performance of the solar energy utilization, on a solar air heating system and on a photovoltaic (PV) system, to power a drying testbench. The objective is to evaluate the efficiency of each system when supplying hot air at certain temperatures at the inlet of a desiccant wheel on the drying system. The testbench is composed of a desiccant wheel, with two separate ducts (process and regeneration) in order to attend the parameters of optimum adsorption at the wheel, in which air heating is provided by a bank of electrical resistances. The energy supply to power the drying system is compared with an off-grid PV system and a flat plate solar collector for air heating. System designs present the required number of PV modules and the solar fraction covered by solar air collector according to the monthly average solar radiation data at Fortaleza, Brazil. The comparison shows that, with a single solar collector from the module described, the solar fraction is 0.73 of the air heating at 50 °C, 0.51 at 71.5 °C and 0.40 at 91 °C.*

Keywords: *drying, desiccant, photovoltaics, solar collector.*

1. INTRODUCTION

Drying is part of a range of important unit operations on global food chain, which ensures food and other material conservation by removing internal water content by means of a temperature and absolute humidity difference between the product and the drying chamber air. This way, the process guarantees an increase of food lifespan and a reduction of post-harvest losses. This represents a challenge facing the population growth paradigm, at which, according to FAO, 2018, humankind could reach 10 billion by 2100. In order to the world food production keep pace, it is necessary to increase by 60% in 2050 the food supply levels of 2005. However, increasing food harvest and transportation efficiency depends on favorable economic and environmental resources. Once that most of the agricultural products are harvested on tropical humid climates – regions with higher probability of microorganism proliferation, the possibility of fungi or bacteria contamination of agricultural products insufficiently dried could affect 4,5 billion people (Bourdoux et al., 2016; Bradford et al., 2017). Thus, it's necessary a drying control on agricultural products.

Recent works present analysis on solar assisted desiccant drying processes and air heating systems. Regenerative methods of desiccant systems and their application on desiccant drying systems were studied (Misha et al., 2012). In papers (Misha et al., 2015) and (Misha et al., 2016) evaluated a solid desiccant dryer assisted by solar energy during kenaf core fiber and palm frond drying. The drying time of the kenaf core fiber was reduced by 24% and the drying rate of the palm frond decreased about 47% on average.

Experiments with a hybrid photothermal infrared (HPIRD) drying system assisted with a desiccant wheel designed and conducted experiments (Punlek et al., 2009). The system mainly consisted of a PV solar air collector, a silica gel desiccant bed and the infrared drying, enabling operation in three modes. HPIRD drying test performance at a temperature of 60 ° C and a speed of 0.6 m/s reduced the drying time by 44% and consumed 63% less energy compared to hot air drying. The hybrid system also produced better dry product quality compared to hot air infrared drying.

Recent work (Slimani et al., 2016) studied a photovoltaic-thermal (PVT) hybrid solar collector configuration incorporated in an indirect solar drying system. The values of electrical, thermal and global energy efficiencies reached 10.5%, 70% and 90%, respectively, with a mass flow rate of 0.0155 kg/s, revealing the importance of the effect of certain parameters and operational conditions in the collector performance results. In papers (Karim and Hawlader, 2004) and (Karim and Hawlader, 2006) a solar air collector was developed and analyzed when noticed the perspective of use on

drying processes. Based on procedures from Klein, Beckman and Duffie, 1977, the authors investigated a design of suitable air collectors as a factor to bring economy of solar drying.

Recently, Ayadi and Al-Dahidi (2019) developed a systematic methodology to compare, technically and economically, solar assisted systems, analyzing the annual energy requirements for solar heating and cooling, but for space and water building systems. This study aims the design and energy optimization of a desiccant drying bench by including PV or/and solar thermal collector system for air heating.

Table 1. Abbreviation list.

Abbreviation	Definition
AC	Alternating Current
CRESESB	Centro de Referência para Energia Solar e Eólica Sérgio Sálvio de Brito (Sérgio Sálvio de Brito Solar and Wind Energy Reference Center)
DC	Direct Current
ESH	Equivalent Sun-Hours
FAO	Food and Agriculture Organization of the United Nations
GTES	Grupo de Trabalho de Energia Solar da CRESESB (Solar Energy Workforce)
HPIRD	Hybrid Photothermal Infrared Radiation Desiccant
INMET	Instituto Nacional de Meteorologia (National Institute of Meteorology)
MPP	Maximum Power Point
PV	Photovoltaic
PVT	Photovoltaic-thermal

2. METHODOLOGY

The section describes the testbench components, listing its operational characteristic and demand. Next, the photovoltaic (PV) and the thermal flat plate solar collector array is analyzed in order to reduce the required power consumption and autonomy of the existing heating system. The procedure is analyzed and discussed in the result section.

2.1 Experimental setup

The experimental drying bench was designed in the form of a tunnel containing control equipment and measuring instrumentation connected to dataloggers. The drying tunnel configuration, shown in Fig. 1, is made of galvanized metal sheet, with 5 mm Styrofoam insulation and with a cross-section internal area of 290 mm wide and 90 mm high. The setup is 3300 mm long (with exhaust section crossing the laboratory external to release the process flow outside), 2025 mm wide and 500 mm high. It has two air duct piping for dehumidification and regeneration - each one with a fan (A), mounted in counterflow and connected to a desiccant wheel (G), with 126 m³/h flow for optimum adsorption, 200 mm diameter and 100 mm rotor thickness mounted after damper and before sample plate. The regeneration duct is mounted above the process duct, with a heating resistance bank (C) before the desiccant wheel. The resistance is responsible for the removal of saturated moisture in rotating silica gel, which is attached to microchannels on the wheel.

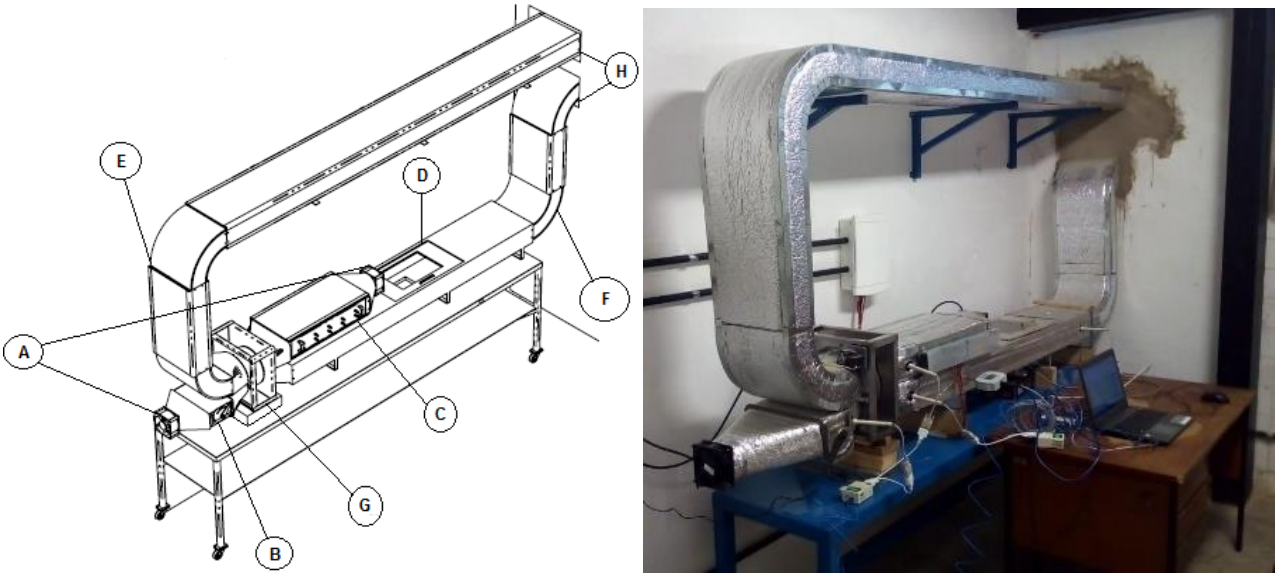

Figure 1. Left: View of experimental testbench arrangement with desiccant wheel and components. Right: Image of the drying system installed. Source: Author.

Thus, the process air duct (F) consists of, as described on the Fig. 2: fan (A), damper (B), desiccant wheel (G), duct with balance (D) and exhaust duct (H).The components of the regeneration air duct (E), on downstream order are: fan (A), heating resistance bank (C), desiccant (G) and exhaust duct (H) – presented on Fig. 3. The objective is to analyze opportunities to absorb solar energy through a PV system or a through a solar air heating system with flat plate collectors. Figure 2 represents the flat plate solar air heating system and an auxiliary heater and Fig. 3 shows the configuration with PV-powered system.

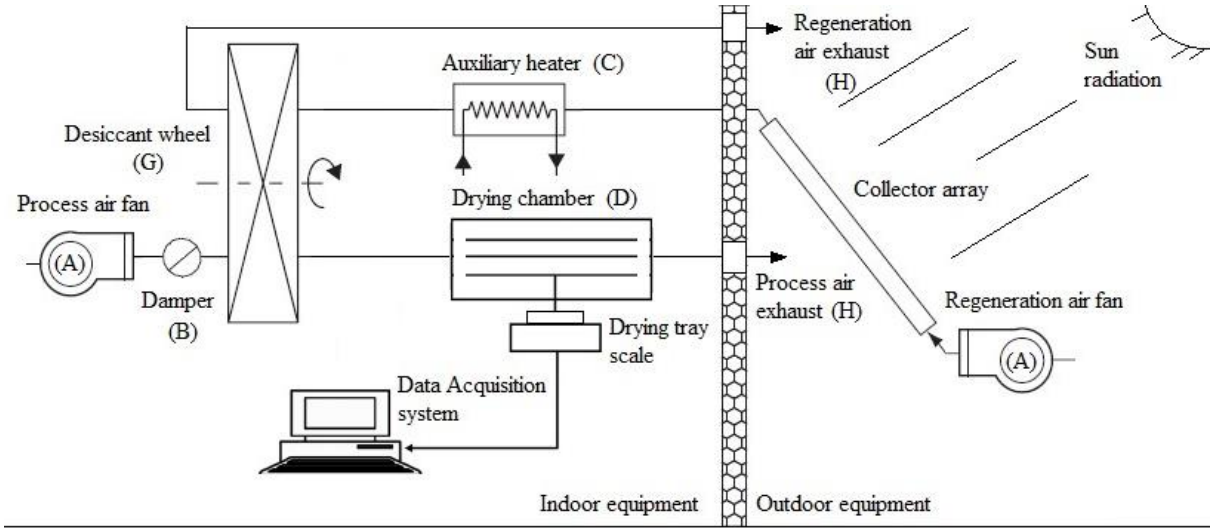

Figure 2. Schematic diagram of the experimental drying system with desiccant wheel regenerated by a solar air collector. Source: Author.

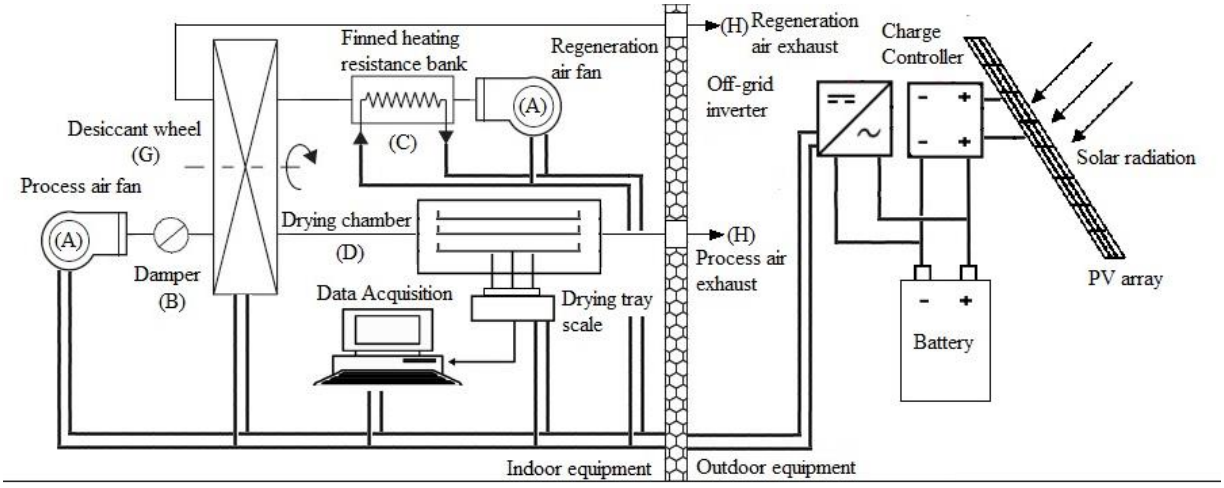

Figure 3. Schematic diagram of the experimental drying system powered by an off-grid PV system. Source: Author.

2.2 Photovoltaic system sizing

In this section, the PV system design is presented following the recommendations of the "Engineering Manual for Photovoltaic Systems" of GTES, 2014. The design fluxogram, as shown in Fig. 4, according to Jäger *et al*., 2014, is summarized in components calculation phases. An off-grid or grid-tie system design starts with the energy consumption amount, when it is necessary to estimate the energy demand according to required autonomy, as shown at Table 2.

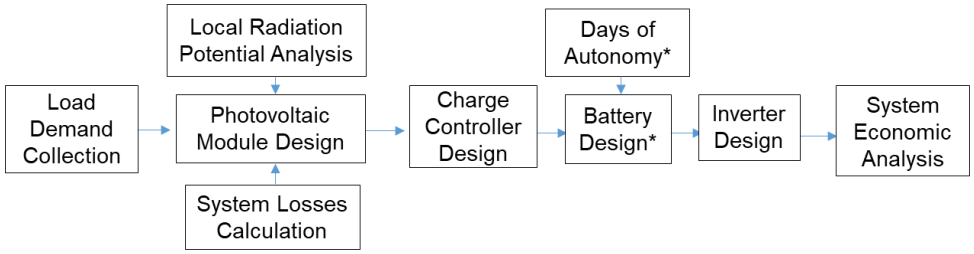

Figure 4. PV system design fluxogram, for off-grid application. Source: adapted from Jäger *et al*., 2014.

The autonomy of the drying testbench depends on drying curve required time, specifically the conditions to achieve moisture equilibrium of the sample moisture with the process air. Prognostics on PV design are dependent on drying process efficiency and the material studied, in this case three scenarios of outlet air temperature from the resistance heating and drying time are analyzed. The first scenario is defined with 50°C dry-bulb temperature for a 6-hour drying, the second one with 71.5°C for drying operation of 3.3 hours, and the third case set with 91°C and 4 hours of drying.

Table 2. Installed power requirement of the experimental bench for the drying process modes

Experimental Bench with Desiccant Wheel			
Item	Quantity	Power per unit (W)	Total Power (W)
Resistance	1	1000	1000
Desiccant wheel	1	1.8	1.8
Blower	2	16	32
Notebook (with anemometer)	1	100	100
Relative humidity and temperature sensors	2	48	96
Balance	1	7.5	7.5
Total			1237.3

The total energy demand for the panels array is calculated considering the DC and AC demands to off-grid and to grid-tie systems. Energy losses related to cable, charge controller, battery and inverter are calculated in order to obtain the actual power demand that the system can operate. Using radiation data from latitude and longitude (Souza, 2017), the monthly average incident radiation is given at Table 3. For off-grid application, the lowest radiant month approach is used, when load demand is covered by the worst scenario of daily conversion rate. In this case, April is the month most

affected in terms of Equivalent Sun Hours (ESH). With this information, the required number of panels is calculated considering the module specification (short-circuit current, open-circuit voltage and peak power), minimum output power and ESH.

Table 3. Monthly average incident radiation at horizontal surface. Source: Souza, 2017.

Fortaleza, Brazil - Latitude: 3.718° S / Longitude: 38.543 °W												
Month	Jan	Feb	Mar	Apr	May	Jun	Jul	Aug	Sep	Oct	Nov	Dec
kW/m²	0.74	0.72	0.64	0.60	0.67	0.68	0.74	0.83	0.86	0.87	0.82	0.79
ESH	5.74	5.54	5.04	4.76	5.17	5.26	5.70	6.42	6.76	6.92	6.56	6.22

In off-grid systems, the configuration of the inverter, load controller and battery are necessary to match with PV array depending on the array voltage and current. The charge controller is responsible for preventing battery power overload damage and reverse current flow from full battery bank at no conversion. The battery arrangement is balanced by system operating voltage and battery nominal voltage, capacity, depth of discharge and the back-up time. The off-grid inverter sizing, responsible to transform DC energy from PV array into AC demand onward, was carried out through equipment nominal specification and, for grid-tie systems, considering nominal voltage and current and minimum power.

2.3 Solar air collector sizing

To reduce the heating resistance bank usage, with a high electricity consumption, during the drying testbench operation, a solar air heater is designed to provide a pre-heated air. The solar fraction of the regeneration air heating is the goal of the design procedure. The starting point is to obtain the heat useful gain according to the temperature required, which is

$$Q_u = \dot{m}.\ C_p\ .\ (T_o - T_a) \tag{1}$$

Where C_p is the air specific heat, T_o is the outlet temperature from the solar air collector and the regeneration inlet air temperature $T_{reg,in}$, established in this case by the drying scenarios on the section 2.2, T_a is the outdoor air temperature obtained through the annual average hourly measurements from the local meteorological station (INMET, 2019) – Tab. 4, $\dot{m}$ is the air mass flowrate in kg/s, defined by

$$\dot{m} = \frac{\dot{V}}{\upsilon} \tag{2}$$

Where υ is the air specific volume, obtained through a psychrometric chart according to the drying testbench sensor measurements and $\dot{V}$ is the air volumetric flowrate – 0.035 m³/s from the nominal flowrate according to the desiccant wheel manufacturer.

Table 4. Maximum, minimum and mean month average incident radiation on hour basis and temperature data collected at meteorological station at Fortaleza. Source: INMET, 2019.

Hour	Incident radiation (kJ/m²)			Temperature (°C)
	Min (May)	Max (Oct)	Average	Average
5	15.22	20.39	9.328128	26.62580645
6	238.40	339.92	231.7693	27.80967742
7	693.81	861.57	753.2588	29.11612903
8	1057.58	1435.91	1214.116	30.03448276
9	1432.68	2026.36	1674.774	30.9
10	1667.31	2575.23	2090.261	31.17333333
11	1812.64	2858.47	2343.15	31.18275862
12	1910.42	2792.41	2369.329	30.73666667
13	1735.26	2429.53	2158.542	30.12580645
14	1413.42	1970.55	1820.573	29.3
15	1087.44	1455.13	1357.347	28.14516129

16	543.42	781.51	737.7196	27.00645161
17	39.02	93.35	124.4738	26.71935484

By comparing the solar energy heat useful gain for a given solar heating system (Duffie and Beckman, 2013). The useful energy gain of a solar collector is

$$Q_u = A_C \,.\, F_R[G_T(\tau\alpha) \; - U_L \,.\, (T_i - T_a)] \tag{4}$$

where A_C is the absorber plate area, F_R is the collector heat removal factor, I_T is the incident solar radiation on the plate – obtained by INMET, 2019, at Tab. 4; $(\tau\alpha)$ is the transmittance-absorptance product dependent on cover material, U_L is the overall heat transfer coefficient, T_i and T_a are the inlet air temperature and ambient temperature, respectively.

The air solar heater used on this study is the v-corrugated collector analyzed by Karim and Hawlader, 2006, with black-painted mild steel as the absorber plate material, fiberglass wool in the back insulation, polystyrene and silicon rubber on the side insulation – Fig. 5.

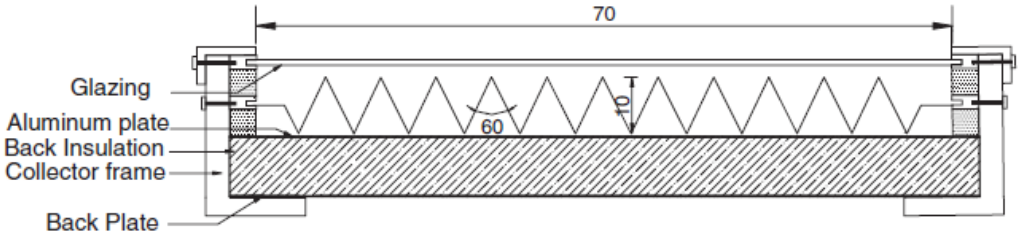

Figure 5. Cross-sectional view of the solar air collector utilized on the comparison. Source: Karim and Hawlader, 2006.

And the parameters used on the solar air collector sizing are given by Tab. 5, with $F_R(\tau\alpha)$ and $F_R U_L$ obtained from efficiency curves developed by Karim and Hawlader, 2006, according to the air mass flowrate range corresponding to the nominal desiccant wheel flowrate.

Table 5. V-corrugated solar air collector design parameters. Source. Karim and Hawlader, 2006.

Parameter	Value	Unit
Mass flowrate ($\dot{m}$)	0.038	kg/s
Specific heat (C_p)	1.02	kJ/(kg.K)
Collector tilt (β)	10	°
Heat removal factor and overall loss coefficient product $F_R U_L$	5.58	W/(m².°C)
Heat removal factor and absorptance-reflectance product $F_R(\tau\alpha)$	0.65	
Length (L)	1.8	M
Width (W)	0.7	M
Height (H)	0.08	M
Efficiency (η)	0.63	

The collector efficiency is given by (Duffie and Beckman, 2013):

$$\eta = \frac{Q_u}{I_T \,.\, A_c} = F_R(\tau\alpha) - \frac{F_R U_L}{(T_i - T_a)} \tag{5}$$

The efficiency found by Karim and Hawlader, 2006, determines the collector inlet air temperature. Through Eq. (1), it is compared with the outlet air temperature. The load fraction carried by solar energy f in daily basis represents how much the solar heating cover the total heating process and defining the use of the resistance bank into an auxiliary heater when the solar incident radiation reduces due to the weather. It is represented by $f = Q_u / L$, in which L means load demand.

$$f = Q_u / L = T_{o,solar} / T_{reg,in} \quad (6)$$

3. RESULTS

The PV system design results for all given scenarios in the month with the lowest Equivalent Sun Hour monthly average (April), as seen on Tab. 6, are detailed with the components used on the Tabs. 7, 8, 9 and 10, and the solar fraction covered by solar air heating covered at Tab. 10, with autonomy given by the scenarios. The PV panel design shows the necessary array installed capacity ranging from 1.96 to 3.08 kW with different PV module solutions (280 and 260 Wp) of 13 options compared according to the PV module cost.

Table 6. PV system sizing results for drying system scenarios.

Drying system configuration	Scenario A	Scenario B	Scenario C
Regeneration inlet air temperature (°C)	50	71.5	91
PV array installed power capacity (kW)	3.08	1.96	1.96
Daily consumption (kWh)	8.33	5.11	5.33
PV module peak power (Wp)	280	260	280
PV module number	11	8	7
Charge controller quantity	1	1	1
Inverter rated power (W)	2860	2000	2000
Inverter number	1	1	1
Battery quantity	6	4	4

Table 7. Selected PV modules characteristics.

Technical specification of the photovoltaic modules utilized		
Model	Yingli Solar YL280P-29b	Canadian Solar CS6P-260P
Peak power (Wp)	280	260
Short-circuit voltage (A)	9.45	8.43
Open-circuit voltage (V)	38.2	37.4
MPP voltage (V)	31.4	30.2
Voltage coefficient (mV/ºC)	-0.32	-0.34
Module area (m²)	1.637	1.608
Conversion efficiency (%)	17.10	16.16

Table 8. Selected off-grid inverters characteristics.

Off-grid inverter technical specification		
Model	EPEVER IP2000-22	MS4448PAE
Rated Power (W)	2000	2860
Max input voltage (V_{dc})	40	64
Max input current (A_{dc})	148	36
Output voltage (V_{ac})	220	120 ~ 240
Efficiency (%)	95	85

Table 9. Selected charge controller characteristics.

Off-grid charge controller technical specification	
Model	Xantrex C40
Voltage configuration (V_{dc})	24
PV module max open-circuit voltage (V_{dc})	125
Max current (A_{dc})	85

Table 10. Selected battery characteristics.

Battery technical specification	
Model	Moura 12MF220
Hour rate regime	20

Depth of discharge	40%
Nominal voltage (V_{dc})	12
Capacity (A.h)	220

For a collector design, the distribution of solar fraction scenarios is shown on an hour basis at Fig. 6. Also, the monthly average, maximum and minimum solar fraction are presented on Tab. 10. Solar fraction ranges from 0,38 to 0,75 according to the scenario and the month of the year. The theoretical maximum outlet collector air temperature varies from 41.5 °C to 47.4 °C. The arrangement, although not covering fully the demand for the drying system, plays a significant role in reducing consumption.

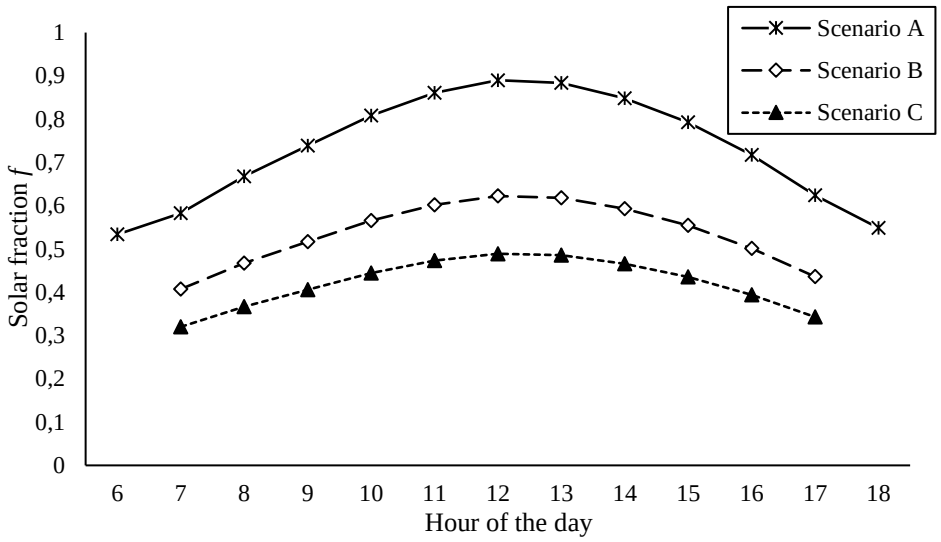

Figure 6. Annual average of solar fraction of the regeneration inlet air heating on hour basis. Source: Author.

Table 11. Solar fraction of the solar air collector on the regeneration inlet temperature

Configuration	Scenario A (50 °C)	Scenario B (71.5 °C)	Scenario C (91 °C)
Minimum monthtly mean f (May)	0.70	0.49	0.39
Annual mean f	0.73	0.51	0.40
Maximum monthly mean f (October)	0.75	0.53	0.41

Considering the minimum, annual and maximum mean solar fraction for each scenario drying time, the outlet temperature of the solar collectors are found through Eq. (1), rearranged to find T_o with inlet temperature T_i obtained from Eq. (4), mass flowrate $\dot{m}$ and C_p provided from Tab. 5. Results are given at Tab. 12.

Table 12. Mean outlet collector temperature for the drying scenarios and throughout the year

Configuration	Scenario A (50 °C)	Scenario B (71.5 °C)	Scenario C (91 °C)
Minimum mean outlet collector temperature T_o (May) (°C)	40.01	41.24	40.92
Annual mean outlet collector temperature T_o (°C)	42.37	43.92	43.53
Maximum mean outlet collector temperature T_o (October) (°C)	44.45	46.61	45.94

In order to achieve the scenario temperatures, it is necessary to use the resistance bank as an auxiliary heater. The auxiliary heat useful gain is calculated with Eq. (1) using the difference between the temperature scenarios (A, B and C)

and mean outlet solar air collector temperature T_o, given by Tab. 12. Table 13 shows the average heat useful gain necessary to meet drying requirements.

Table 13. Additional heat useful gain on the regeneration inlet temperature

Configuration	Scenario A (50 °C)	Scenario B (71.5 °C)	Scenario C (91 °C)
Minimum monthtly mean Q_{aux} (May) (kW)	0.39	1.17	1.94
Annual mean Q_{aux} (kW)	0.29	1.07	1.84
Maximum monthly mean Q_{aux} (October) (kW)	0.22	0.96	1.75

Tables 11, 12 and 13 show that a single collector module cannot provide entirely the required inlet air temperature, but reduces in, at least, 40% the electricity cost to power the heating resistance bank – as seen on scenario C at Tab. 12. Also, this heat consumption is affected by the month of the year, with difference of 200 W from the lowest to the highest incident radiation month in the scenario C. The necessary drying time is important to achieve higher mean temperatures if centered at the noon, the highest average is obtained by the scenario B as shown at Tab. 12, once that this configuration requires only 3 hours of operation. Larger drying operations show larger difference due to radiation sinusoidal profile during the day – Tab. 4.

4. CONCLUSIONS

The experimental drying bench design presents different renewable energy supply configuration for PV and solar thermal system, enabling decision-taking tools to intermittent conditions to reduce energy consumption or to cover demand supply on standalone application. The autonomy of desiccant drying system is dependent of the material to be dried, but it is only feasible if it represents enough time economy to overcome energy consumed by conventional systems.

The arrangement, although not covering fully the demand for the drying system, plays a significant role in reducing consumption. Reducing costs, not only on the supply side, but, also, on the demand side, represents a significant increase in investment rate, however, on a food processing unit production, greater energy efficiency must combine with the time required for batch drying and the solar radiation availability for solar air collectors.

5. ACKNOWLEDGEMENTS

The authors would like to thank the National Council for Scientific and Technological Development (CNPq) for the partial financial support with Universal Process No. 445968-2014-1 through a research project, and the Brazilian Coordination for the Improvement of Higher Education Personnel (CAPES) for the Master´s student assistantship.

6. REFERENCES

Ayadi, O., Al-Dahidi, S., 2019. "Comparison of solar thermal and solar electric space heating and cooling systems for buildings in different climatic regions". *Solar Energy*. Vol. 188, pp. 545-560.

Bourdoux, S., Li, D., Rajkovic, A., Devlieghere, F., Uyttendaele, M. 2016. "Performance of drying technologies to ensure microbial safety of dried fruits and vegetables". *Comprehensive Reviews in Food Science and Food Safety*. Vol. 15, pp. 1056-1066.

Bradford, K. J., Dahal, P., van Asbrouck, J., Kunusoth, K., Bello, P., Thompson, J., WU, F., 2017. "The dry chain: reducing postharvest losses and improving food safety in humid climates". *Trends in Food Science & Technology*, Vol. 71, pp. 84-93.

Duffie, J.A., Beckman, W.A., 2013. *Solar Engineering of Thermal Process*. John Wiley & Sons, New Jersey, 4th edition.

FAO, 2018. *Food loss and waste and the right to adequate food: making the connection.* Rome. 48 pp.

Freire, F.N., 1999. *Experimental setup construction for development of drying curves*. Master Thesis, Universidade Federal do Ceará, Fortaleza, Brazil.

GTES, 2014. *Manual de Engenharia para Sistemas Fotovoltaicos.* Grupo de Trabalho de Energia da CRESESB (Centro de Referência para Energia Solar e Eólica Sérgio de Salvo Brito). Rio de Janeiro, Brazil, 2nd edition.

Jäger, K., Isabella, O., Smets, A. H. M; van Swaaij., R. A. C. M. M., Zeman, M., 2014. *Solar Energy: Fundamentals, Technology and Systems*. Delft University of Technology, Netherlands, 2nd edition.

Karim, A.; Hawlader, M., 2004. “Development of solar air collector for drying applications”. *Energy Conversion and Management*. Vol. 45, pp. 329-344.

Karim, A.; Hawlader, M., 2006. “Performance evaluation of a V-groove solar air collector for drying applications”. *Applied Thermal Engineering*. Vol. 26. pp. 121-130.

Klein, S.A., Beckman, W.A., Duffie, J.A., 1976. "A design procedure for solar air heating systems". *Solar Energy*. Vol. 19, pp. 509-512.

INMET, 2019. “Estação Meteorológica de Observação de Superfície Automática” Instituto Nacional de Meteorologia. 1 Jul. 2019 < http://www.inmet.gov.br/portal/index.php?r=estacoes/estacoesAutomaticas>.

Misha, S., Mat, S., Ruslan, M. H., Salleh, E., Sopian, K., 2012. “Review of solid/liquid desiccant in the drying applications and its regeneration methods”. *Renewable and Sustainable Energy Reviews*. Vol. 16, pp. 4686-4707.

Misha, S., Mat, S., Ruslan, M. H., Salleh, E., Sopian, K., 2015. “Performance of a solar assisted solid desiccant dryer for kenaf core fiber drying under low solar radiation”. *Solar Energy*. Vol. 112, pp. 194–204.

Misha, S., Mat, S., Ruslan, M. H., Salleh, E., Sopian, K., 2016. “Performance of a solar assisted solid desiccant dryer for oil palm fronds drying”. *Solar Energy*. Vol. 132, pp. 415–429.

Punlek, C., Pairintra, R., Chindaraksa, S., Maneewan, S., 2009. “Simulation design and evaluation of hybrid PV/T assisted desiccant integrated HA-IR drying system (HPIRD)”. *Food and Bioproducts Processing*. Vol. 87, pp. 77-86.

Slimani, M. E. A., Amirat, M., Bahria, S., Kurucz, I., Aouli, M., Sellami, R., 2016. “Study and modeling of energy performance of a hybrid photovoltaic/thermal solar collector: configuration suitable for an indirect solar dryer”. *Energy Conversion and Management*. Vol. 125, pp. 209-221.

Souza, L.J.S., 2017. *Especificação de uma bancada de secagem com ligação à rede elétrica por sistema fotovoltaico*. Monography, Universidade Federal do Ceará, Fortaleza, Brazil.

7. RESPONSIBILITY NOTICE

The authors are the only responsible for the printed material included in this paper.